Terahertz photoconductivity of mobile electrons in nanoporous InP honeycombs

J. Lloyd-Hughes,[1,*] S. K. E. Merchant,[1] L. Sirbu,[2] I. M. Tiginyanu,[2] and M. B. Johnston[1,†]
[1]*Department of Physics, Clarendon Laboratory, University of Oxford, Parks Road, Oxford OX1 3PU, United Kingdom*
[2]*National Center for Materials Study and Testing, Technical University of Moldova, and Institute of Applied Physics, Academy of Sciences of Moldova, Chisinau MD-2004, Republic of Moldova*
(Received 8 June 2008; published 26 August 2008)

Nanostructured semiconductors with favorable optoelectronic properties can be created by electrochemical etching, a fabrication process that is scalable for mass market applications. Using terahertz photoconductivity measurements, we demonstrate that nanoporous InP has an unusually long carrier recombination lifetime that exceeds 100 ns at low temperatures and low carrier density, and an electron mobility half that of bulk InP. Modeling confirms that these observations result from band bending with holes confined to the surface and electrons away from the pores.

DOI: 10.1103/PhysRevB.78.085320 PACS number(s): 73.63.−b, 78.47.jc, 73.61.Ey

Materials and devices with tailored optoelectronic properties can be created by structuring semiconductors on nanometer length scales. For instance, field-effect transistors[1] and single-photon detectors[2] have been made from semiconductor nanowires[3] while nanoporous membranes[4] show promise as nonlinear optical materials.[5,6] In order to create operable devices from nanomaterials, the doping level of the semiconductor must be controlled accurately. However, surface and interfacial states can significantly alter the charge transport properties of nanodevices, creating charge depletion or accumulation layers[7] and capacitive effects.[8] It is highly desirable to investigate the influence of surface states on the conductivity of nanomaterials particularly via noncontact techniques.

The frequency-dependent complex conductivity $\sigma(\omega)=\sigma_1(\omega)+i\sigma_2(\omega)$ of many bulk inorganic semiconductors is well described by the Drude model of free-carrier absorption, in which the real part of the conductivity σ_1 decreases with frequency and the imaginary part σ_2 is positive.[9] Substantially different conductive responses can be found when carriers are localized within nanometer-sized structures: σ_2 can be negative and may change sign above a characteristic resonant frequency, above which it remains positive. Terahertz time-domain spectroscopy[10] has been used to measure σ of nanostructures directly and a variety of responses have been observed. For instance, excitonic resonances are seen in GaAs quantum wells at low temperature[11–13] while in GaAs nanowires at room temperature, the conductivity is indicative of surface plasmons.[14] The terahertz conductivity of quantum dots remains controversial and different models have been used to describe the system: free-carrier absorption within the Bruggeman effective-medium theory,[15] the excitonic dielectric function,[16] and extensions of the Drude model that consider carrier backscattering at surfaces.[17–19] Additionally, in amorphous semiconductors, the lack of long-range order can result in the conductivity obeying power laws $\sigma \propto \omega^n$ at frequencies from the megahertz to terahertz ranges,[20,21] which can be explained theoretically within Mott's variable-range hopping model of localized carriers.

Here we report the terahertz photoconductivity of nanostructured InP containing an axially aligned, dense array of pores ~60 nm in diameter. The observed complex conductivity perpendicular to the pores is consistent with free-carrier absorption despite the amorphous nature of the pore array and the nanometer length scales of the semiconductor. We find this to be true across our experimental temperature and fluence range. The observed mobility is roughly half that of bulk InP at the same doping level. Via simulations of the band structure and carrier distribution, we attribute the bulk-like properties of nanoporous InP to surface pinning of the chemical potential, which depletes the regions close to the pores of electrons.

The electrochemical etching of ⟨111⟩-oriented InP (n doped at 10^{18} cm^{-3}) was performed in order to generate curro pores perpendicular to the surface.[4] Samples were characterized by scanning electron microscopy (Fig. 1), and were found to have a mean pore diameter of ~60 nm and an interpore spacing of 110 nm. Cross-sectional micrographs confirmed that the pores ran through the ~30 μm thickness of each nanoporous film. Samples were mounted in the variable-temperature insert of a cryostat, enabling measurements at lattice temperatures between 1.8 and 100 K (limited by the signal-to-noise ratio at high temperature). A terahertz time-domain spectrometer similar to that described in Ref. 22 was used to measure the photoconductivity under excitation at 800 nm with pulses 100 fs in duration at an 80 MHz repetition rate. The incident terahertz radiation was linearly polarized and probed the conductivity perpendicular to the axes of the pores. As the hole effective mass in bulk InP is substantially larger than the electron effective mass, we assumed that the measured conductivity originated from photoexcited electrons only.

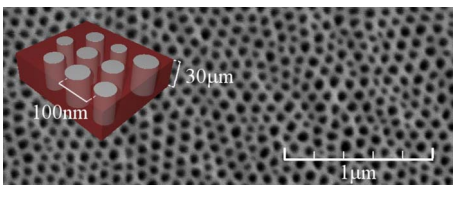

FIG. 1. (Color online) Scanning electron micrograph of the surface of ⟨111⟩-oriented nanoporous InP. The inset shows a three-dimensional (3D) cartoon of the pores, which run through the ~30 μm thickness of the samples. The conductivity at terahertz frequencies was measured in the plane of the surface, perpendicular to the pores.

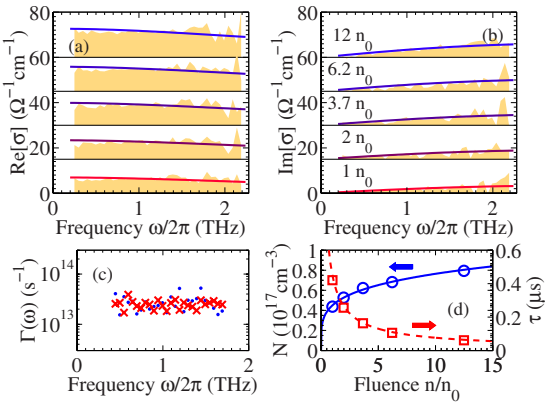

FIG. 2. (Color online) [(a) and (b)] Shaded areas show the measured (a) real and (b) imaginary parts of the photoexcited conductivity of nanoporous InP at a lattice temperature of 40 K at various incident fluences ranging from $n_0=6.0\times10^{10}$ cm^{-2} to $12n_0$. Solid lines are fits using the Drude conductivity of a free-electron gas [Eq. (2)]. (c) $\Gamma(\omega)$ calculated from Eq. (3) at fluences of n_0 (points) and $12n_0$ (crosses). (d) Electron density extracted from the fits to the Drude conductivity (circles) and calculated carrier lifetime (squares). The solid line ($N\propto n_0^{0.23}$) and dashed line ($\tau\propto n_0^{-0.77}$) are guides to the eye.

The measured conductivity was not observed to alter with pump-probe delay time both before and after the arrival of the pump pulse at "zero delay." This suggests that the carrier recombination lifetime τ in nanoporous InP is long in comparison to the laser repetition period ($\Delta t=12.5$ ns). In the limit $\tau\gg\Delta t$, a simple rate equation yields the equilibrated photoinduced charge density N as

$$N=N_0\frac{\tau}{\Delta t}, \tag{1}$$

where N_0 is the carrier density generated by a single pulse. The photoexcited carrier density can therefore be enhanced substantially above N_0, depending on τ. We calculated N_0 at each pump fluence from the measured pump spot size, power, and absorption depth at 800 nm of InP. Equation (1) is used later to calculate τ from N determined from the frequency-dependent conductivity.

In Figs. 2(a) and 2(b) the real and imaginary parts of the photoconductivity are plotted at various incident pump fluences for a lattice temperature of 40 K. Considering the data at the lowest fluence (bottom shaded areas), σ_1 is positive throughout the frequency range and decreases weakly with frequency. The imaginary part of σ is positive and increases with frequency. These trends are reproduced well by the Drude model of free electrons, as shown by the solid lines. In this model the complex conductivity can be written as

$$\sigma(\omega)=\frac{Ne^2(i\omega+\Gamma)}{m^*(\omega^2+\Gamma^2)}, \tag{2}$$

where N, e, and m^* are, respectively, the density, charge, and effective mass of electrons in the material (we assume that $m^*=0.08m_e$, the bulk value for InP). Γ is the electron momentum scattering rate, which is assumed to be independent of frequency in the Drude model. It can be seen readily from Eq. (2) that Γ is given by

$$\Gamma=\omega\frac{\sigma_1(\omega)}{\sigma_2(\omega)}. \tag{3}$$

This means that the electron momentum scattering rate can be calculated directly as a function of frequency from the experimental $\sigma(\omega)$. Any frequency dependence to $\Gamma(\omega)$ would immediately invalidate the Drude approach.

In Fig. 2(c) $\Gamma(\omega)$ is shown as calculated from the experimental $\sigma(\omega)$ using Eq. (3) at the lowest and highest fluence. No frequency dependence to Γ can be resolved, indicating the validity of the Drude approach, and the scattering rate is also independent of pump fluence. The obtained value of $\Gamma=2.7\times10^{13}$ s^{-1} corresponds to an electron mobility $\mu\simeq814$ cm^2 V^{-1} s^{-1}, almost half that of bulk InP ($\mu\sim2000$ cm^2 V^{-1} s^{-1}) at a similar doping level and temperature.[23] The corresponding mean-free path for electrons is 6 nm, smaller than the narrowest width of the semiconductor honeycomb ($\sim$50 nm), and thus surface scattering only weakly affects the mobility. This finding is consistent with the high mobility of GaAs nanowires recently reported.[14]

At high pump-laser fluence the spectral shape of the conductivity remains similar to that at low fluence [Figs. 2(a) and 2(b)]. The change in the photoexcited electron density N with pump fluence n is shown in Fig. 2(d), as obtained from fits using Eq. (2), with the value of Γ fixed to that in Fig. 2(c). We also calculate the recombination lifetime τ at each pump fluence from the fitted N using Eq. (1). At low fluence, $\tau\sim400$ ns, a value much longer than that which we directly measure for bulk InP (300 ps). Larger recombination times are often seen when electron-hole recombination is suppressed by charge separation, for instance, in *nipi* superlattices.[24] The photoexcited electron density N increases sublinearly with fluence, which can be attributed to a reduction in τ due to an enhanced electron recombination rate. The origin of this effect is discussed below in conjunction with a simulation of the material's electronic structure.

Furthermore, we have measured the conductivity of nanoporous InP at lattice temperatures from 1.8 up to 100 K (limited by the obtainable signal). The frequency dependence of σ is consistent with the Drude conductivity over this temperature range. In Fig. 3 we show the momentum scattering time $1/\Gamma$ [obtained from Eq. (3)] as a function of temperature. At higher lattice temperatures the mobility $\mu=e/(\Gamma m^*)$ decreases slightly, ruling out a thermally activated transport mechanism such as the two-dimensional (2D) variable-range hopping relation $\mu\propto\exp[(T_0/T)^{-1/3}]$.[25] This is further evidence that the nanoscale pores do not appear to hinder bulklike semiconductor transport.

As a comparison, the scattering time for bulk 10^{18} cm^{-3} n-type InP is also plotted in Fig. 3, taken from Hall mobility measurements.[23] The scattering rate for bulk InP is also not strongly temperature dependent as a result of carrier-impurity scattering dominating the mobility.[23] In contrast, the scattering time for semi-insulating InP (circles) displays a peak in $1/\Gamma$ at 80 K. This is a characteristic of less heavily doped polar semiconductors when at high tem-

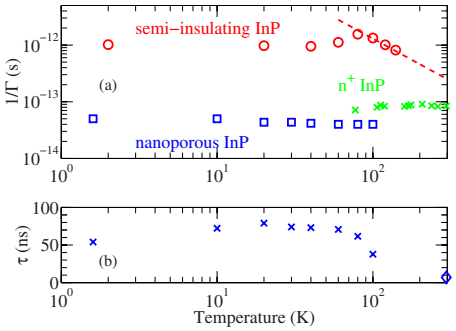

FIG. 3. (Color online) (a) The temperature dependence of the carrier momentum scattering time $1/\Gamma$ is shown at an incident fluence of $12n_0$ for nanoporous InP (squares) and bulk n-type InP at a comparable doping level (crosses, from Hall mobilities in Ref. 23). Also shown is $1/\Gamma$ measured for semi-insulating InP (circles). The dashed line indicates the temperature dependence of the mobility from TO-phonon scattering, $\mu \propto T^{-3/2}$. (b) The recombination lifetime τ of photoexcited carriers in nanoporous InP (crosses), obtained from Eq. (1), utilizing fits to the complex conductivity as in Fig. 2(d). The value of τ at 296 K (diamond) was measured under photoexcitation using pulses from an amplified laser (Ref. 26).

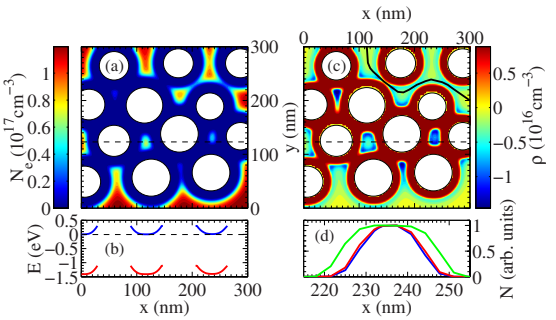

FIG. 4. (Color online) Carrier density of nanoporous InP at 100 K, simulated as described in the text. (a) Electron density without photoexcitation over a 300×300 nm^2 area. The electron density is depleted close to the pores (white circles). The horizontal dotted line indicates the cross section taken in the plot of the band structure (b), in which the conduction and valence bands are shown relative to the Fermi level ($E=0$). (c) Charge density ρ under photoexcitation at $\Delta N = 10^{17}$ cm^{-3}. The negative regions away from the pores represent higher electron density; the solid line shows a conductive pathway. (d) Normalized photoinduced change in electron density in a region along the cross section at $\Delta N = 10^{16}$, 10^{17}, and 10^{18} cm^{-3} (from inner to outer lines).

peratures carrier-phonon scattering ($\mu \propto T^{-3/2}$, dashed line) dominates.[27]

In order to investigate the nanoscale physics of porous semiconductors theoretically, we used a self-consistent Schrödinger-Poisson solver[28] to calculate the two-dimensional carrier density and band structure in thermal equilibrium at 100 K. We used an n-type doping of 1.0×10^{18} cm^{-3} throughout the nanoporous material with a donor level of 6 meV below the conduction band.[29] At the semiconductor surface, we assumed that the Fermi level was pinned 0.3 eV above its value in bulk, a typical value for InP surfaces.[30] One-dimensional solutions to the Schrödinger-Poisson equation indicated that the electron density was at most 4% different from that obtained upon neglecting quantum effects and, therefore in our 2D simulations, we solved the Poisson equation only. To represent the actual structure (Fig. 1), we modeled the pores as a pseudorandom array of circles with mean diameter of 60 nm and interpore spacing of 110 nm, shown by the white circles in Fig. 4.

The simulated electron density and band structure of nanoporous InP are shown in Figs. 4(a) and 4(b). The equilibrium electron density can be seen to be strongly depleted close to the pores (white circles). This results from the pinning of the Fermi level at the surface, which bends the electronic bands upward, as Fig. 4(b) illustrates for a cross section through the pores. Within ~20 nm of the pores, the conduction band is raised higher above the chemical potential (at 0 eV in this figure), creating an electron depletion layer. The spacing between pores is often comparable to the depletion width, resulting in the large depletion regions seen in Fig. 4(a). This electron depletion accounts for the good terahertz transmission through our nanoporous InP samples, which would otherwise be opaque owing to the 10^{18} cm^{-3} n-doping concentration and ~30 μm thickness. Substantial electron density can occur only in regions where the nearest pore is at a distance greater than approximately 20 nm.

In our simulation we introduced an extra donor density $\Delta N = 10^{17}$ cm^{-3} in order to model the effect of photoexcitation in nanoporous InP. The immobile ionized donors are analogous to the low-mobility photogenerated hole population. In Fig. 4(c) the difference in charge density between this simulation and the equilibrium charge density is shown. Photoexcited electrons reside in the regions of large negative charge density, away from the pores, while excess positive charge is seen around the pores. Pathways for electrical conduction can be seen along regions where the pores are further separated, as indicated by the solid line in Fig. 4(c). The maximum photoinduced electron density is of the order of 10^{16} cm^{-3}, as a result of the strong electron depletion regions.

The electronic structure reported in Fig. 4 can account for the observed features of the terahertz-frequency photoconductivity. The regions of high electron density [~20 nm, Fig. 4(d)] are larger than the mean-free path (7 nm at 100 K), and the conductivity should therefore have a frequency and temperature dependence similar to that of free electrons in bulk InP, as indeed we observed (Figs. 2 and 3). Photoexcited electrons and holes are separated spatially, as the charge density in Fig. 4(c) indicates, which reduces radiative recombination and accounts for the long lifetimes reported herein. We performed simulations at different photoinjected carrier densities and plot the obtained photoinduced electron density in Fig. 4(d) for a region of the porous material. At $\Delta N = 10^{18}$ cm^{-3} the maximum photoinduced electron density was 10^{17} cm^{-3}, comparable to the experimental density [Fig. 2(d)]. Increasing ΔN from 10^{16} to 10^{18} cm^{-3} makes the electron distribution broader as a result of a flattening of the conduction band. This enhances the overlap of the electron and hole wave functions, creating a larger radiative recombination rate and reducing the recombination lifetime τ. This effect qualitatively explains the shortening in τ at higher pump-laser fluence shown in Fig. 2.

The measured temperature dependence of τ is also shown in Fig. 3 and was obtained as described above with reference to Fig. 2(d). Toward higher temperatures, τ can be seen to decrease, which can be interpreted as follows. At low temperatures the photoexcited holes are confined close to the surface, the electron-hole separation is large, and the radiative recombination rate is therefore low. At higher temperatures, holes obtain sufficient thermal energy to escape the surface, increasing the recombination rate.

Finally, the regions of electrostatically confined electrons are small enough to generate quantum confinement effects, which can enhance the binding energy of excitons. However, no excitonic resonance in the conductivity was observed here, in contrast to previous spectroscopic studies of other nanostructures, for instance GaAs quantum wells.[31] This may be a result of our measurement technique averaging over regions with different sizes and therefore binding energies: the excitonic oscillator strength would then be dispersed spectrally.

We have reported herein that photoexcited nanoporous InP exhibits the frequency- and temperature-dependent conductivities of a free-electron gas with a mobility approaching that of bulk InP but a substantially longer carrier lifetime. Via two-dimensional simulations, we attribute this to charge separation within the nanoporous structure. Our findings highlight the important influence that surface states have on conduction in nanoscale semiconductors. The precise control of surface states is likely to be critical to the functionality of nanoelectronic devices.

The authors would like to acknowledge financial support from the EPSRC-GB (UK) and from INTAS under Grant No. 05–104–7567.

*Present address: ETH Zürich, Institute for Quantum Electronics, Wolfgang-Pauli-Strasse 16, 8093 Zürich, Switzerland. james.lloyd-hughes@phys.ethz.ch

†m.johnston@physics.ox.ac.uk

[1] Y. Cui, Z. H. Zhong, D. L. Wang, W. U. Wang, and C. M. Lieber, Nano Lett. **3**, 149 (2003).

[2] A. Fujiwara, K. Yamazaki, and Y. Takahashi, Appl. Phys. Lett. **80**, 4567 (2002).

[3] M. Law, J. Goldberger, and P. D. Yang, Annu. Rev. Mater. Res. **34**, 83 (2004).

[4] H. Föll, S. Langa, J. Carstensen, M. Christophersen, and I. M. Tiginyanu, Adv. Mater. (Weinheim, Ger.) **15**, 183 (2003).

[5] I. M. Tiginyanu, I. V. Kravetsky, J. Monecke, W. Cordts, G. Marowsky, and H. L. Hartnagel, Appl. Phys. Lett. **77**, 2415 (2000).

[6] M. Reid, I. Cravetchi, R. Fedosejevs, I. M. Tiginyanu, L. Sirbu, and R. W. Boyd, Phys. Rev. B **71**, 081306(R) (2005).

[7] K. I. Seo, S. Sharma, A. A. Yasseri, D. R. Stewart, and T. I. Kamins, Electrochem. Solid-State Lett. **9**, G69 (2006).

[8] S. A. Dayeh, C. Soci, P. K. L. Yu, E. T. Yu, and D. L. Wang, Appl. Phys. Lett. **90**, 162112 (2007).

[9] D. Grischkowsky, S. Keiding, M. van Exter, and C. Fattinger, J. Opt. Soc. Am. B **7**, 2006 (1990).

[10] C. A. Schmuttenmaer, Chem. Rev. (Washington, D.C.) **104**, 1759 (2004).

[11] R. H. M. Groeneveld and D. Grischkowsky, J. Opt. Soc. Am. B **11**, 2502 (1994).

[12] R. A. Kaindl, M. A. Carnahan, D. Hagele, R. Lovenich, and D. S. Chemla, Nature (London) **423**, 734 (2003).

[13] J. Lloyd-Hughes, H. E. Beere, D. A. Ritchie, and M. B. Johnston, Phys. Rev. B **77**, 125322 (2008).

[14] P. Parkinson, J. Lloyd-Hughes, Q. Gao, H. H. Tan, C. Jagadish, M. B. Johnston, and L. M. Herz, Nano Lett. **7**, 2162 (2007).

[15] M. C. Beard, G. M. Turner, and C. A. Schmuttenmaer, Nano Lett. **2**, 983 (2002).

[16] F. Wang, J. Shan, M. A. Islam, I. P. Herman, M. Bonn, and T. F. Heinz, Nat. Mater. **5**, 861 (2006).

[17] N. V. Smith, Phys. Rev. B **64**, 155106 (2001).

[18] G. M. Turner, M. C. Beard, and C. A. Schmuttenmaer, J. Phys. Chem. B **106**, 11716 (2002).

[19] D. G. Cooke, A. N. MacDonald, A. Hryciw, J. Wang, Q. Li, A. Meldrum, and F. A. Hegmann, Phys. Rev. B **73**, 193311 (2006).

[20] P. Lunkenheimer and A. Loidl, Phys. Rev. Lett. **91**, 207601 (2003).

[21] H. Harimochi, J. Kitagawa, M. Ishizaka, Y. Kadoya, M. Yamanishi, S. Matsuishi, and H. Hosono, Phys. Rev. B **70**, 193104 (2004).

[22] J. Lloyd-Hughes, S. K. E. Merchant, L. Fu, H. H. Tan, C. Jagadish, E. Castro-Camus, and M. B. Johnston, Appl. Phys. Lett. **89**, 232102 (2006).

[23] W. Walukiewicz, J. Lagowski, L. Jastrzebski, P. Rava, M. Lichtensteiger, C. H. Gatos, and H. C. Gatos, J. Appl. Phys. **51**, 2659 (1980).

[24] M. B. Johnston, M. Gal, G. Li, and C. Jagadish, J. Appl. Phys. **82**, 5748 (1997).

[25] N. Mott, Rev. Mod. Phys. **50**, 203 (1978).

[26] S. K. E. Merchant, J. Lloyd-Hughes, L. Sirbu, I. M. Tiginyanu, P. Parkinson, L. M. Herz, and M. B. Johnston, Nanotechnology **19**, 395704 (2008).

[27] P. Y. Yu and M. Cardona, *Fundamentals of Semiconductors*, 3rd ed. (Springer, New York, 2003).

[28] NEXTNANO, http://www.wsi.tum.de/nextnano3/

[29] *Handbook Series on Semiconductor Parameters* (World Scientific, Singapore, 1996), Chap. 7.

[30] J. S. Hwang, W. Y. Chou, M. C. Hung, J. S. Wang, and H. H. Lin, J. Appl. Phys. **82**, 3888 (1997).

[31] B. Gerlach, J. Wusthoff, M. O. Dzero, and M. A. Smondyrev, Phys. Rev. B **58**, 10568 (1998).